5th International Conference on
Electrical and Computer Engineering
With emphasis on native knowledge
ieeec.ir
February , 2018 , Tehran-Iran

Comparison of SVM and RF Algorithms for Crop Mapping Using Bi-Temporal Optical and Radar Data with Limited Training Samples

Iman Khosravi[1,*] Saeid Niazmardi[2], Abdolreza Safari[1], Saeid Homayouni[3]
[1]School of Surveying and Geospatial Engineering, College of Engineering, University of Tehran, Tehran, I.R. Iran
[2]Faculty of Civil & Surveying Engineering, Graduate University of Advanced Technology, Kerman, I.R. Iran
[3]Department of Geography, Environment, and Geomatics, University of Ottawa, Ottawa, Canada

ABSTRACT

This paper aims to compare two state-of-the-art classification algorithms, namely Support Vector Machine (SVM) and Random Forest (RF) algorithms, in terms of accuracy and running time, in order to crop mapping from multi-temporal optical and radar images with limited training samples. The optical data are RapidEye images and the radar data are UAVSAR images. The case study is an agricultural area near Winnipeg, Manitoba, Canada. From each RapidEye image, 38 optical features, and from each UAVSAR image, 49 radar features were extracted. The results indicated RF was more efficient in the classification of radar features, while SVM was more efficient in the classification of optical and stacked features. Furthermore, regarding running time, RF was much faster than SVM in all scenarios.

Keywords: support vector machine, random forest, crop mapping, optical image, radar image

1. INTRODUCTION

Optical and Radar satellites are two important sources of Remote Sensing and Earth Observation technologies for crop mapping [1]. A variety of invaluable features can be extracted from both sources. From optical satellites, various spectral bands, vegetation indices (VIs) and textural indicators can be generated and extracted. These features give information about reflectance behaviour or spatial arrangement of gray levels which have exclusive capabilities in discriminating various crop types [2]. Among the optical sensors, RapidEye has an additional spectral channel, i.e., Red-Edge (RE). In some recent studies, several additional vegetation indices has been defined based on this band which are proved very useful for discriminating vegetation and various crop types [3].

By contrast, the most important parameters of synthetic aperture radar (SAR) satellites are complex polarization observations (intensity and phase data) which offer information about the physical and structural properties of land covers. In addition, an especial type of SAR sensors, i.e., full-polarimetric SAR (PolSAR) sensor are recently widely used for crop mapping and monitoring. Compared to single- and multi-polarized SAR sensors, the PolSAR sensors such as UAVSAR offer a more variety of parameters, such as polarimetric discriminators and target decompositions. These features can provide vital information about scattering mechanisms of different types of crop [4].

Each of optical or radar imagery has some exclusive defects; the optical sensors are usually limited by weather and atmospheric effects. By contrast, the PolSAR sensors may be faced with speckle defect and other geometrical errors such as radar shadows, layover and foreshortening. The fusion of these two sources can offer a complementary data source, which is free of shortcomings of both. In fact, either represents a unique point of view. For example, for crop mapping, passive optical energy reflected by vegetation depends on leaf structure, dye, and moisture. By contrast, active microwave energy scattered by vegetation is dependent on the size, density, orientation, and dielectric characteristics of elements comparable to the size of the radar wavelength [5]. Furthermore, multi-time fusion of optical and radar imagery can often provide more inestimable and more dependable information than single-time fusion [1].

In this work, we aim to dedicate on crop mapping from temporal observations of RapidEye and UAVSAR images acquired on 2012, 5th and 14th July, over an agricultural area near Winnipeg, Manitoba, Canada. Seven crop types can be defined in this region which have the imbalanced distributions. The main objective of this paper is to compare two state-of-the-art classification algorithms with limited training samples in a high-dimensional optic-radar feature space, in terms of accuracy, and running time. These algorithms are Support Vector Machine (SVM) as a widely used representative of kernel-based methods family and Random Forest (RF) as a favourable representative of ensemble systems family. From each RapidEye image, 38 optical features, such as spectral bands, vegetation indices based on red

and RE channels, and textural indicators, and from each UAVSAR image, 38 radar features such as polarization intensities, polarization ratios, polarization correlations, and target decompositions were extracted.

2. DATASET AND STUDY AREA

The study area of this paper was the southwest district of Winnipeg, Manitoba, Canada covered from various agriculture crops (see Figure 1). The area of the region is near 100 Hectares and its mean elevation from sea-level is 724 meters. This region was the site study of Soil Moisture Active Passive Mission (SMAP) prelaunch field campaign (SMAPVEX 2012) [6]. Seven classes could be defined in this region as follows: Canola, Corn, Soybeans, Pease, Oats, Wheat and Broadleaf. The number of samples for each class is shown in Table 1. In this paper, 0.5%, 1%, and 3% of all samples were randomly stratified selected for training and remaining were considered for evaluating the algorithms.

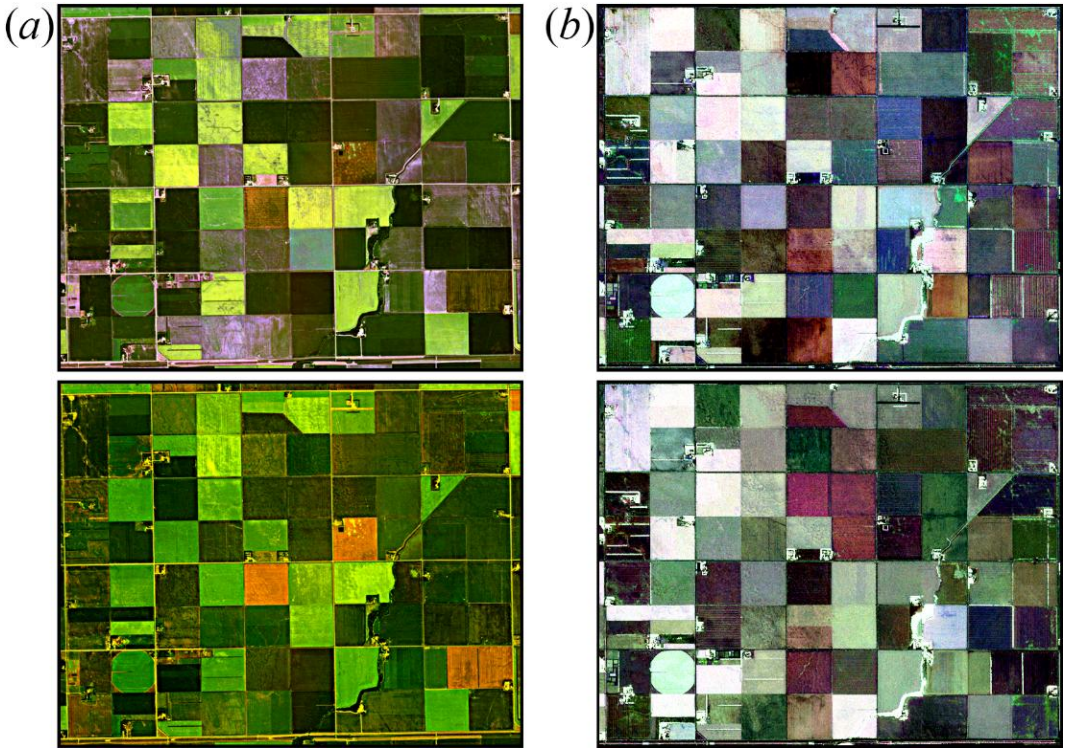

Fig. 1. Remote sensing data used in this paper: (a) RGB color of RapidEye images (R, G, B), (b) Pauli RGB color of UAVSAR images (R: |HH–VV|, G: 2|HV|, B: |HH+VV|). Top: 5th July 2012, Bottom: 14th July 2012.

Table 1. Number of all samples for the study area

Classes	Corn	Peas	Canola	Soybeans	Oats	Wheat	Broadleaf
Number of samples	39162	3598	75673	74067	47117	85074	1143

The data used in this paper were the temporal observations of RapidEye and UAVSAR images. They were acquired at two dates, 5th July 2012 and 14th July 2012. RapidEye images had five spectral channels including blue (B), green (G), red (R), near infrared (NIR) and Red-Edge (RE) and their spatial resolution was 5 meters. UAVSAR images were acquired in L-band and had four polarizations. Their spatial resolution after pre-processing, i.e., multi-looking (2x3) and de-speckling using refined Lee filter, was approximately 15 meters.

The features extracted from each RapidEye image were the spectral channels, some well-known vegetation indices, and textural indicators based on gray-level occurrence matrix (Kross et al., 2015). They were totally 38 features presented in Table 2. In addition, 49 polarimetric features, including polarization intensities and ratios, polarization correlation coefficients, Eigenvalue decompositions, and coherent and incoherent decomposition parameters were extracted from each UAVSAR image (Tamiminia et al., 2017). They are presented in Table 3.

Table 2. The optical features extracted from the RapidEye images

Blue (B)	440-510 nm
Green (G)	520-590 nm
Red (R)	630-685 nm
Red-Edge (RE)	690-730 nm
Near Infrared (NIR)	760-850 nm
Normalized Difference Vegetation Index	$NDVI = (NIR - R)/(NIR + R)$
Simple Ratio	$SR = NIR / R$
Red-Green Ratio Index	$RGRI = G / R$
Enhanced Vegetation Index	$EVI = 2.5 \times (NIR - R)/(NIR + 6R - 7.5B + 1)$
Atmospherically Resistant Vegetation Index	$ARVI = (NIR - (2R - B))/(NIR + (2R - B))$
Soil Adjusted Vegetation Index	$SAVI = (1 + L) \times (NIR - R)/(NIR + R + L); L = 0.5$
Normalized Difference Greenness Index	$NDGI = (G - R)/(G + R)$
Green NDVI	$gNDVI = (NIR - G)/(NIR + G)$
Modified Triangular Vegetation Index	$MTVI2 = 1.5 \times (1.2 \times (NIR - G) - 2.5 \times (R - G))/\sqrt{(2 \times NIR + 1)^2 - (6 \times NIR - 5 \times \sqrt{R}) - 0.5}$
Red Edge Normalized Difference Vegetation Index	$NDVIre = (NIR - RE)/(NIR + RE)$
Red Edge Simple Ratio	$SRre = NIR / RE$
Red Edge Normalized Difference Greenness Index	$NDGIre = (G - RE)/(G + RE)$
Red-edge triangular vegetation index	$RTVIcore = 100 \times (NIR - RE) - 10 \times (NIR - G)$
Red Edge NDVI	$RNDVI = (RE - R)/(RE + R)$
Transformed CARI	$TCARI = 3 \times ((RE - R) - 0.2 \times (RE - G)(RE / R))$
Triangular Vegetation Index	$TVI = 0.5 \times (120 \times (RE - G) - 200 \times (R - G))$
Red Edge Ratio 2	$PRI2 = RE / R$
μ_{PC1}, σ_{PC1}, HOM_{PC1}	μ_{PC2}, σ_{PC2}, HOM_{PC2}
CON_{PC1}, DIS_{PC1}, H_{PC1}	CON_{PC2}, DIS_{PC2}, H_{PC2}
ASM_{PC1}, COR_{PC1}	ASM_{PC2}, COR_{PC2}

Table 3. The radar features extracted from the UAVSAR images

$\sigma_{hh} = 10\log\lvert S_{hh}\rvert^2$, $\sigma_{hv} = 10\log\lvert S_{hv}\rvert^2$, $\sigma_{vv} = 10\log\lvert S_{vv}\rvert^2$, $\sigma_{rr} = 10\log\lvert S_{rr}\rvert^2$, $\sigma_{rl} = 10\log\lvert S_{rl}\rvert^2$, $\sigma_{ll} = 10\log\lvert S_{ll}\rvert^2$
$R_{hhvv} = 10\log(\lvert S_{hh}\rvert^2/\lvert S_{vv}\rvert^2)$, $R_{hvhh} = 10\log(\lvert S_{hv}\rvert^2/\lvert S_{hh}\rvert^2)$, $R_{hvvv} = 10\log(\lvert S_{hv}\rvert^2/\lvert S_{vv}\rvert^2)$,
$R_{rrll} = 10\log(\lvert S_{rr}\rvert^2/\lvert S_{ll}\rvert^2)$, $R_{rlrr} = 10\log(\lvert S_{rl}\rvert^2/\lvert S_{rr}\rvert^2)$, $R_{rlll} = 10\log(\lvert S_{rl}\rvert^2/\lvert S_{ll}\rvert^2)$
$R_{hh} = 10\log(\lvert S_{hh}\rvert^2/SPAN)$, $R_{hv} = 10\log(\lvert S_{hv}\rvert^2/SPAN)$, $R_{vv} = 10\log(\lvert S_{vv}\rvert^2/SPAN)$
$R_{rr} = 10\log(\lvert S_{rr}\rvert^2/SPAN)$, $R_{rl} = 10\log(\lvert S_{rl}\rvert^2/SPAN)$, $R_{ll} = 10\log(\lvert S_{ll}\rvert^2/SPAN)$
$\rho_{hhvv} = \lvert\langle S_{hh}.S_{vv}^*\rangle/\sqrt{\langle S_{hh}.S_{hh}^*\rangle\langle S_{vv}.S_{vv}^*\rangle}\rvert$ $\rho_{rrll} = \lvert\langle S_{rr}.S_{ll}^*\rangle/\sqrt{\langle S_{rr}.S_{rr}^*\rangle\langle S_{ll}.S_{ll}^*\rangle}\rvert$ $\rho_{hvhh} = \lvert\langle S_{hv}.S_{hh}^*\rangle/\sqrt{\langle S_{hv}.S_{hv}^*\rangle\langle S_{hh}.S_{hh}^*\rangle}\rvert$
$\rho_{rlrr} = \lvert\langle S_{rl}.S_{rr}^*\rangle/\sqrt{\langle S_{rl}.S_{rl}^*\rangle\langle S_{rr}.S_{rr}^*\rangle}\rvert$ $\rho_{hvvv} = \lvert\langle S_{hv}.S_{vv}^*\rangle/\sqrt{\langle S_{hv}.S_{hv}^*\rangle\langle S_{vv}.S_{vv}^*\rangle}\rvert$ $\rho_{rlll} = \lvert\langle S_{rl}.S_{ll}^*\rangle/\sqrt{\langle S_{rl}.S_{rl}^*\rangle\langle S_{ll}.S_{ll}^*\rangle}\rvert$
$\lambda_1, \lambda_2, \lambda_3, H = -\sum_{i=1}^{3} p_i \log_3 p_i$ $\{p_i = \lambda_i / \sum_{k=1}^{3} \lambda_k\}$, $A = (\lambda_2 - \lambda_3)/(\lambda_2 + \lambda_3)$, $\overline{\alpha} = \sum_{i=1}^{3} p_i \alpha_i$, $HA, H(1-A), (1-A)H, (1-H)(1-A)$
$\psi = \min(\lambda_1, \lambda_2, \lambda_3)/(\lambda_1 + \lambda_2 + \lambda_3)$, $RVI = 4 * \lambda_3/(\lambda_1 + \lambda_2 + \lambda_3)$
$\lvert\alpha\rvert^2 = \lvert(S_{hh} + S_{vv})/\sqrt{2}\rvert^2$, $\lvert\beta\rvert^2 = \lvert(S_{hh} - S_{vv})/\sqrt{2}\rvert^2$, $\lvert\gamma\rvert^2 = 2\lvert S_{hv}\rvert^2$, $\lvert k_s\rvert^2 = \lvert S_{rl}\rvert^2$, $\lvert k_d\rvert^2 = \min(\lvert S_{rr}\rvert^2, \lvert S_{ll}\rvert^2)$, $\lvert k_h\rvert^2 = abs(\lvert S_{rr}\rvert^2 - \lvert S_{ll}\rvert^2)$
$P_s = f_s(1 + \lvert\beta\rvert^2)$, $P_d = f_d(1 + \lvert\alpha\rvert^2)$, $P_v = f_v$, $P_s^Y = f_s(1 + \lvert\beta\rvert^2)$, $P_d^Y = f_d(1 + \lvert\alpha\rvert^2)$, $P_v^Y = f_v$, $P_c^Y = f_c$

3. METHODOLOGY

Two state-of-the-art classification algorithms, i.e. Support vector machine (SVM) and random forest (RF) were used in this paper for classification task. They are as follows:

3.1 Support vector machine

SVM is a binary supervised learning algorithm, which maps the data into a high dimensional space, in which the data have simpler (more linear) representation. This mapping is done implicitly by using a kernel function. After mapping, the SVM estimates a separating hyperplane between two classes in the kernel space, so that it has the maximum distance from the nearest samples of each class. The position of the samples with respect to this separating hyperplane is then used for their classification. For multi-class task, SVM uses either of one-against-one or one-against-

all strategies. The most widely used kernel function is radial basis function (RBF) kernel which has two main parameters: penalty parameter (C) and Gaussian width parameter (σ) [7].

3.2 Random forest

RF combines a multitude of diverse decision trees (DT) in order to reduce the risk of over-fitting. RF trains the DTs separately as parallel. This algorithm injects randomness into two steps of the training process as follows: dividing the training samples into several subsamples (nTrees) by a random-with replacement-sampling method, called as bootstrapping method; considering a subset of features (mTry) from all features for each subsample by a random-without replacement-feature selection method, called as random subset feature selection method. In prediction process for a test sample, RF assigns a wining class which receives the highest number of votes by the DTs [8].

4. RESULTS AND DISCUSSION

All the implementations were carried out on a Windows 10 64 bit system with Intel® Core™ i7 Q740 CPU and 30GB of RAM by MATLAB 2015. In this section, SVM and RF algorithms were used for classification of three scenarios, i.e., scenario1: radar features, scenario2: optical features, and scenario3: combination of radar and optical features. For SVM, RBF kernel function was utilized. For obtaining its optimum values, a grid search procedure by cross validation was used with the intervals of [10-2:0.5:101], and [0.1:100:2000] for C and γ, respectively. In addition, out-of-bag (OOB) error was used for optimizing the RF parameters. The interval of [5, 10:10:100, 200:100:1000] was considered for *n*Trees. For *m*Try, the round of the square root of all features in each scenario was considered.

Table 4. Accuracy results of the methods

			SVM	RF
Percent = 0.5%	*Scenario 1*	OA	67.63	72.27
		Kappa	0.59	0.69
		F-score Mean	0.68	0.69
	Scenario 2	OA	61.10	61.25
		Kappa	0.56	0.57
		F-score Mean	0.52	0.50
	Scenario 3	OA	80.21	77.24
		Kappa	0.75	0.74
		F-score Mean	0.74	0.72
Percent = 1%	*Scenario 1*	OA	72.78	78.05
		Kappa	0.69	0.75
		F-score Mean	0.70	0.74
	Scenario 2	OA	71.09	70.38
		Kappa	0.68	0.67
		F-score Mean	0.61	0.59
	Scenario 3	OA	87.46	81.93
		Kappa	0.84	0.79
		F-score Mean	0.83	0.78
Percent = 3%	*Scenario 1*	OA	80.86	81.18
		Kappa	0.76	0.78
		F-score Mean	0.79	0.80
	Scenario 2	OA	80.99	79.19
		Kappa	0.76	0.76
		F-score Mean	0.73	0.70
	Scenario 3	OA	90.23	85.89
		Kappa	0.88	0.83
		F-score Mean	0.88	0.83

For the comparison of the methods, overall accuracy (OA), kappa coefficient, F-score, and running time were considered. The OA is a general metric for the evaluation of the classification and is the ratio of the diagonal pixels to

the all samples of the confusion matrix. The kappa coefficient is computed to determine whether the values in a confusion matrix are significantly better than the values in a random assignment. The F-score is the harmonic mean of producer's and user's accuracies of each class and can offer a realistic assessment of the classification compared to the OA and the kappa [9, 10]. Table 4 presents the accuracy results of the methods, and Figure 2 demonstrates the time plot of the methods in three percent and three scenarios.

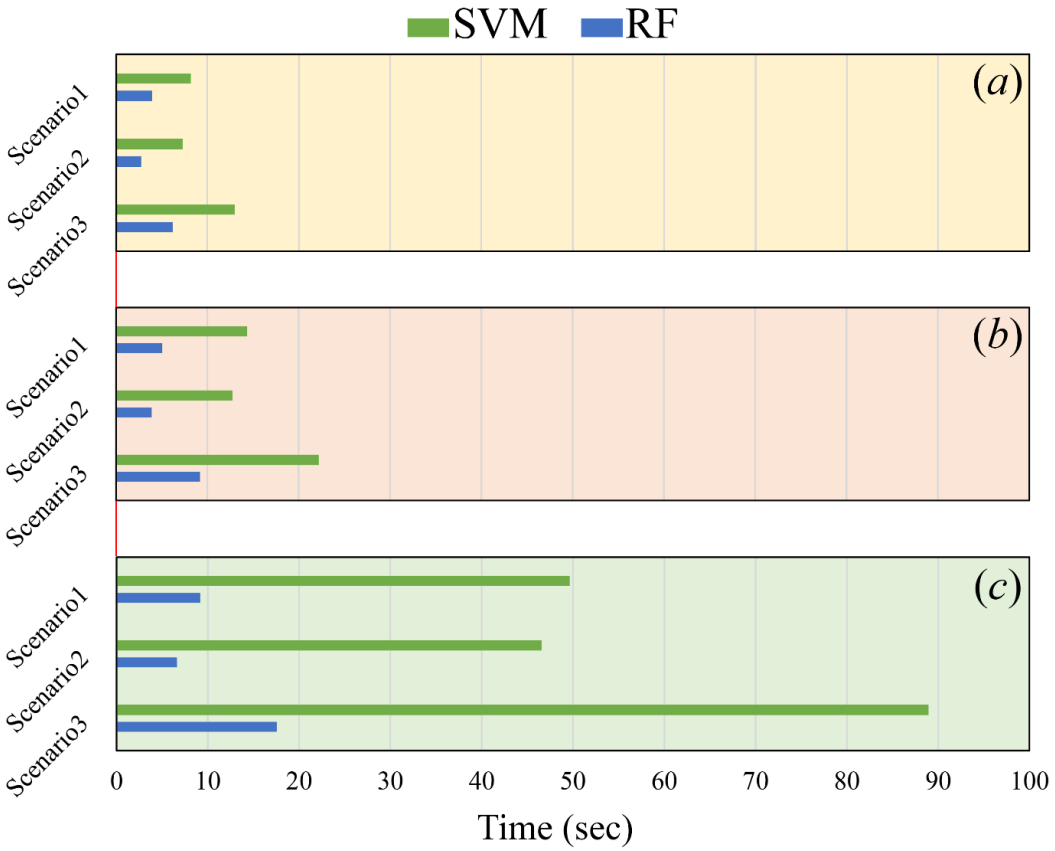

Fig. 2. Time plots of the SVM and RF methods for three scenarios 1 (radar features), 2 (optical features), and 3 (combination of radar and optical features) with three training sizes: (a) 0.5%, (b) 1%, and (c) 3%.

From Table 4, one could be seen that the RF algorithm has obtained higher OA, kappa coefficient, and F-score mean values than the SVM in the classification of the radar features (scenario 1) with all three training sizes. The difference differs from 2% (at the size of 3%) to 6% (at the size of 1%) for the OA values. By contrast, the SVM has obtained higher OA, kappa, and F-score mean values than the RF in the classification of the optical features (scenario 2) with the sizes of 1% and 3%. Of course, the difference was few (about 1%) compared to the former. However, in the classification of scenario 3, i.e. the stacked radar and optical features, the SVM has also higher accuracies than the RF with three sizes. The difference was between 3% (at the size of 0.5%) and 6% (at the size of 3%) for the OA values.

Regarding running time, including optimization, model generation, and classification times, Figure 2 indicated that the RF algorithm was faster than the SVM in all three scenarios with three training sizes. It's noteworthy that the larger training size was, the much faster performance for the RF compared to the SVM was obtained. Figures 2a and 2b demonstrated the 2 and 3 times more speediness of the RF, and Figure 2c indicated the 5 and 7 times more speediness of the RF compared to the SVM.

An important note regarding the results is that the best performance of the RF algorithm in all three scenarios was obtained using the data without normalization. By contrast, for the SVM in all scenarios, the data was normalized between zero and 1 in order to achieve best results of the SVM. This fact implies that feature scaling is although very important for the SVM efficiency, it may degrade the RF efficiency.

5. CONCLUSION

This paper evaluated and compared support vector machine (SVM) and random forest (RF) algorithms for crop mapping from a fused radar and optical data with thee limited training samples. We concluded that the RF was more efficient than the SVM for the classification of radar features, while the SVM was more efficient for the classification of optical features, and stacked radar and optical features. Meanwhile, the RF was much faster than the SVM with all three training sizes.

ACKNOLEDGEMENT

The authors would like to thank the JPL NASA, the SMAPVEX 2012 team, and the Agriculture and Agri-Food for providing the PolSAR and optical data used in this paper.

REFERENCES

[1] McNairn, H., Champagne, C., Shang, J., Holmstrom, D., Reichert, G. (2009). Integration of optical and Synthetic Aperture Radar (SAR) imagery for delivering operational annual crop inventories. *ISPRS Journal of Photogrammetry and Remote Sensing*, vol. 64, no. 5, p. 434-449.

[2] Peña-Barragán, J.M., Ngugi, M.K., Plant, R.E., Six, J. (2011). Object-based crop identification using multiple vegetation indices, textural features and crop phenology. *Remote Sensing of Environment*, vol. 115, no. 6, p. 1301-1316.

[3] Kross, A., McNairn, H., Lapen, D., Sunohara, M., Champagne, C. (2015). Assessment of RapidEye vegetation indices for estimation of leaf area index and biomass in corn and soybean crops. *International Journal of Applied Earth Observation and Geoinformation*, vol. 34, p. 235-248.

[4] Tamiminia, H., Homayouni, S., McNairn, H., Safari, A. (2017). A particle swarm optimized kernel-based clustering method for crop mapping from multi-temporal polarimetric L-band SAR observations. *International Journal of Applied Earth Observation and Geoinformation*, vol. 58, p. 201-212.

[5] Khosravi, I., Safari, A., Homayouni, S. (2018). MSMD: maximum separability and minimum dependency feature selection for cropland classification from optical and radar data, *International Journal of Remote Sensing*, DOI: 10.1080/01431161.2018.1425564

[6] McNairn, H., Jackson, T.J., Wiseman, G., Belair, S., Berg, A., Bullock, P., Colliander, A., Cosh, M.H., Kim, S.-B., Magagi, R., Moghaddam, M. (2015). The soil moisture active passive validation experiment 2012 (SMAPVEX12): Prelaunch calibration and validation of the SMAP soil moisture algorithms. *IEEE Transactions on Geoscience and Remote Sensing*, vol. 53, no. 5, p. 2784-2801.

[7] Niazmardi, S., Shang, J., McNairn, H., Homayouni, S. (2013). A new classification method based on the support vector regression of NDVI time series for agricultural crop mapping. *In Agro-Geoinformatics (Agro-Geoinformatics), 2013 Second International Conference on*, p. 361-364.

[8] Khosravi, I., Safari, A., Homayouni, S., McNairn, H. (2017). Enhanced decision tree ensembles for land-cover mapping from fully polarimetric SAR data. *International Journal of Remote Sensing*, vol. 38, no. 3, p. 7138-7160.

[9] Congalton, R.G. (1991). A review of assessing the accuracy of classifications of remotely sensed data. *Remote Sensing of Environment*, vol. 37, no. 1, p. 35-46.

[10] Powers, D.M. (2011). Evaluation: from precision, recall and F-measure to ROC, informedness, markedness & correlation. *Journal of Machine Learning Technologies*, vol. 2, no. 1, p. 37-63.